THIN FILM SILICON SOLAR CELL PREPARED BY THERMAL EVAPORATION ON POLYIMIDE SUBSTRATE

MOHD ZAMIR BIN PAKHURUDDIN

UNIVERSITI SAINS MALAYSIA

2012

THIN FILM SILICON SOLAR CELL PREPARED BY THERMAL EVAPORATION ON POLYIMIDE SUBSTRATE

by

MOHD ZAMIR BIN PAKHURUDDIN

Thesis submitted in fulfilment of the requirements
for the degree of
Master of Science

February, 2012

ACKNOWLEDGEMENT

Firstly, thanks to Allah for giving me a chance to complete this research and thesis. I would like to express my sincere gratitude to my main supervisor, Professor Kamarulazizi bin Ibrahim for his valuable guidance and continuous support throughout the course of this project. I would also like to thank my co-supervisor, Dr Azlan bin Abdul Aziz for his kind assistance in this research.

Thanks to Universiti Sains Malaysia (USM) and Ministry of High Education (MOHE) of Malaysia for sponsoring my studies on Academic Staff Training Scheme (ASTS) programme (under School of Physics). Again, thanks to Universiti Sains Malaysia (USM) for providing a research grant 1001/PFIZIK/821061 for this project.

Much of this work would have been virtually impossible without the technical support from Nano-Optoelectronics Research and Technology Laboratory (N.O.R) staffs; Mr. Mohtar Sabdin, Mrs. Ee Bee Choo, Mr. Hazhar Hassan, Mr. Abdul Jamil Yusuf and Mr. Aswafi. Also thanks to my fellow friends; Marzaini, Ghaffar, Khalil, Anas, Yushamdan, Siti Khadijah, Zaki, Mahayatun and others (not mentioned here) who have given me useful advices throughout this research.

Finally, I would like to thank my dearest wife, Nur Adelina binti Ahmad Noruddin for her constant motivation, support and patience during the whole research and thesis writing processes. Not to forget my beloved children; Muhammad Haiqal and Nur Iman Balqis for cherishing my life all this while.

TABLE OF CONTENTS

Acknowledgement		ii
Table of Contents		iii
List of Tables		vii
List of Figures		viii
List of Abbreviations		xvi
List of Symbols		xix
Abstrak		xxi
Abstract		xxiii
CHAPTER 1 - INTRODUCTION		
1.1	Solar Energy	1
1.2	Efficiency and Cost Projections of Solar Technologies	4
1.3	Problem Statement	6
1.4	Scope of Research	8
1.5	Objectives of Research	9
1.6	Organisation of Thesis	9
CHAPTER 2 - LITERATURE REVIEW		
2.1	Solar Cells Device Families	11
2.2	Strategies Towards Cost Reduction	14
2.3	Progress in Thin Film Silicon Solar Cells Research	15
	2.3.1 Issues of Thin Film Silicon Solar Cells	15
	2.3.2 Methods and Approaches	17
CHAPTER 3 - THEORY		
3.1	Photovoltaic Effect	25
3.2	Solar Spectrum	26
3.3	Thermal Evaporation	29

3.4 Thin Film Silicon Solar Cells Physics 34
3.4.1 Silicon Material 34
3.4.2 Doping 38
3.4.3 Structure of P-N and P-I-N Junction 40
3.4.4 Absorption, Separation and Transport 44
3.4.5 Light Trapping Mechanisms 51
3.4.6 Solar Cell Equivalent Circuit and Basic Equations 58
3.4.7 Current-Voltage Curve and Efficiency Calculation 61
3.4.8 Ideality Factor 63
3.5 Loss Mechanisms in Thin Film Silicon Solar Cells 65
3.5.1 Optical Losses 67
3.5.2 Recombination Losses 68
3.5.3 Other Losses 70

CHAPTER 4 - MATERIALS AND METHODS

4.1 Deposition Equipments: 72
4.1.1 Thermal Evaporation 72
4.1.2 Radio Frequency (R.F) Sputtering 73
4.2 Annealing Equipment 75
4.3 Characterisation Equipments 74
4.3.1 Thermal Properties of Plastic Substrates 76
4.3.1 (a) Thermogravimetric Analyser (TGA) 76
4.3.1 (b) Differential Scanning Calorimeter (DSC) 76
4.3.2 Structural Properties 78
4.3.2 (a) Optical Reflectometer 78
4.3.2 (b) Energy Dispersive X-Ray (EDX) 79
4.3.2 (c) Raman Spectroscopy 81
4.3.2 (d) High Resolution X-Ray Diffractometer (XRD) 82

4.3.3 Surface Morphology 84
4.3.3 (a) Atomic Force Microscope (AFM) 84
4.3.3 (b) Scanning Electron Microscope (SEM) 85
4.3.4 Electrical Properties 86
4.3.4 (a) Four-Point Probe (Sheet Resistance/Resistivity Measurement System) 86
4.3.4 (b) Hall Effect Measurement System 87
4.3.4 (c) Solar Simulator System 88
4.3.5 Optical Properties 90
4.3.5 (a) Double Beam UV-Visible Spectrophotometer (UV-Vis) 90
4.3.5 (b) Optical Reflectometer 91
4.4 Fabrication and Characterisation of Thin Film Silicon Solar Cells 92
4.4.1 Thermal Properties of Plastic Substrates 92
4.4.2 Structural and Optical Properties of Plastic (Polyimide) Substrate 95
4.4.3 Surface Texturing of Plastic (Polyimide) Substrate 95
4.4.4 Process Flow in Thin Film Silicon Solar Cells Fabrication 97
4.4.5 Current-Voltage Characterisation (Dark and Illuminated) and Efficiency Calculation of Thin Film Silicon Solar Cells 109

CHAPTER 5 - RESULTS AND DISCUSSION

5.1 Properties of Polyimide and Polyethylene Terephthalate 111
5.1.1 Thermal Properties 111
5.1.2 Structural Properties 115
5.1.3 Surface Morphology 116
5.1.4 Optical Properties 117
5.2 Properties of Textured Polyimide Substrates 118
5.2.1 Surface Morphology 118
5.3 Properties of Aluminium Back Contact 122
5.3.1 Structural Properties 122
5.3.2 Surface Morphology 123
5.3.3 Electrical Properties 124

5.3.4 Optical Properties 125
5.4 Properties of P-Type Thin Film Silicon Absorber Layer 128
5.4.1 Structural Properties 128
5.4.2 Surface Morphology 139
5.4.3 Electrical Properties 142
5.4.4 Optical Properties 147
5.5 Properties of Intrinsic Thin Film Silicon Layer 152
5.5.1 Structural Properties 152
5.5.2 Optical Properties 154
5.6 Properties of N-Type Thin Film Silicon Emitter Layer 157
5.6.1 Structural Properties 157
5.6.2 Surface Morphology 159
5.6.3 Electrical Properties 160
5.6.4 Optical Properties 161
5.7 Properties of Zinc Oxide Anti-Reflective Coating (ARC) 162
5.7.1 Structural Properties 162
5.7.2 Surface Morphology 163
5.7.3 Optical Properties 164
5.8 White Paint Back Surface Reflector (BSR) 170
5.8.1 Optical Properties 170
5.9 I-V Characterisation of Thin Film Silicon Solar Cells 171
5.9.1 Illuminated I-V Characteristics 171
5.9.2 Dark I-V Characteristics 181
5.9.3 Overall Thin Film Silicon Solar Cells Performance 185

CHAPTER 6 - CONCLUSION AND RECOMMENDATIONS

6.1 Conclusions 192
6.2 Recommendations for Future Studies 194

REFERENCES 196
LIST OF PUBLICATIONS 207

LIST OF TABLES

		Page
Table 4.1	Fabricated samples of thin film Si solar cells on PI substrates	108
Table 5.1	Summary of electrical properties of Al-doped thin film Si as measured by Hall effect system	142
Table 5.2	Summary of electrical properties of Sb-doped thin film Si on PI as measured by Hall effect system	160
Table 5.3	Summary of efficiencies of microcrystalline thin film Si solar cells on PI substrates with p-n and p-i-n junction configurations, designed with various light trapping techniques. The cells were tested using solar simulator system under 220 W/m^2 illumination under AM1.5 at 25°C (Cells area = 4 cm^2)	173

LIST OF FIGURES

		Page
Figure 1.1	Monocrystalline silicon (c-Si) solar panel	1
Figure 1.2	Cumulative worldwide annual PV installed capacity	2
Figure 1.3	Efficiency and cost projections of three generations of solar technologies (First generation: wafers, Second generation: thin films, Third generation: advanced thin films)	4
Figure 1.4	PV market shares in 2010 (breakdown by technology)	6
Figure 2.1	Monocrystalline (c-Si) solar cell	11
Figure 2.2	The ultimate efficiency limit of solar energy conversion (Landsberg's limit)	13
Figure 2.3	Reduction of substrate (absorber layer) thickness as a potential solution for cost reduction	14
Figure 2.4	PECVD system	19
Figure 2.5	Schematic of Si e-beam evaporation system with boron and phosphorus effusion cells for in-situ doping used in	22
Figure 3.1	Photovoltaic effect in a solar cell	25
Figure 3.2	Spectral irradiance of the sun under AM0 and AM1.5	27
Figure 3.3	The optical path length (air mass) that the sun radiation has to pass through before reaching the earth's surface	28
Figure 3.4	Thermal evaporation system	29
Figure 3.5	Thermal evaporation process	30
Figure 3.6	Vapour pressure of various elements against temperatures	32
Figure 3.7	Schematic illustration for determination of thickness distribution across the substrate	33
Figure 3.8	Schematic representation of covalent bonds in an intrinsic Si crystal lattice	34

Figure 3.9	Types of Si materials: (a) monocrystalline Si (c-Si) (b) multicrystalline (mc-Si) or polycrystalline Si (pc-Si) (c) amorphous Si (a-Si)	35
Figure 3.10	Schematic of energy bands for electrons in a semiconductor	36
Figure 3.11	Limiting conversion efficiency for a single band gap solar cell under AM0 and AM1.5	37
Figure 3.12	Schematic of a Si crystal lattice doped with impurities to produce n-type and p-type Si	38
Figure 3.13	Position of Fermi level (E_F) in: (a) intrinsic Si (b) n-type Si (c) p-type Si	39
Figure 3.14	(a) Schematic diagram of a p-n junction (b) Band diagram of a p-n junction in equilibrium	40
Figure 3.15	(a) Schematic diagram of a p-i-n junction (b) Band diagram of a p-i-n junction in equilibrium	42
Figure 3.16	Photogeneration process (creation of electron-hole pairs) upon illumination with light of energy $E_{ph} > E_g$	44
Figure 3.17	Electron-hole pair generation at different depths of the absorber material by photons of different energies	45
Figure 3.18	Logarithmic plot of absorption coefficient (α) of various semiconductor materials (i.e. absorber layers) at 300 K as a function of wavelength (in nm)	46
Figure 3.19	Optical absorption in direct and indirect band gap semiconductors	48
Figure 3.20	Typical configuration of thin film Si solar cell	49
Figure 3.21	Photogeneration and separation at p-n junction region	50
Figure 3.22	Reflectance of incident light on (a) untextured (smooth) thin film surface (b) textured (rough) thin film surface	53
Figure 3.23	Randomising rear reflector	54
Figure 3.24	Role of quarter-wavelength ($\lambda/4$) ARC to suppress surface reflectance	55

Figure 3.25	Typical reflectance level of Si surface before and after application of quarter-wavelength ARC	57
Figure 3.26	Equivalent circuit of a solar cell	58
Figure 3.27	Sources of series resistance in a solar cell	59
Figure 3.28	Effects of series resistance (R_s) towards I-V curve of a solar cell	59
Figure 3.29	Effects of shunt resistance (R_{sh}) towards I-V curve of a solar cell	60
Figure 3.30	Linear dark and illuminated I-V curve of a solar cell	61
Figure 3.31	Illuminated I-V curve of a solar cell with I_{sc}, I_{max}, V_{oc} and V_{max}	62
Figure 3.32	Loss mechanisms in a solar cell: (1) non-absorption of below band gap photons (2) lattice thermalisation loss (3) and (4) are junction and contact voltage losses (5) recombination loss	65
Figure 3.33	Sources of optical loss in a solar cell	67
Figure 3.34	Main types of recombination	68
Figure 3.35	Shading loss due to shading effect by top metal fingers	70
Figure 3.36	Source of contact resistance loss (interface between metal-semiconductor)	71
Figure 4.1	Thermal evaporation system	72
Figure 4.2	RF sputtering system	74
Figure 4.3	Annealing tube furnace	75
Figure 4.4	TGA system	76
Figure 4.5	DSC system	77
Figure 4.6	Optical reflectometer system	79
Figure 4.7	EDX system integrated to scanning electron microscope (SEM)	79
Figure 4.8	Raman spectroscopy system	81

Figure 4.9	HR-XRD system	83
Figure 4.10	AFM system	84
Figure 4.11	Four-point probe	86
Figure 4.12	Hall effect measurement system	87
Figure 4.13	Solar simulator system	88
Figure 4.14	UV-Vis system	90
Figure 4.15	TGA measurement (PI and PET substrates)	92
Figure 4.16	DSC measurement of PI substrate (in N_2 ambient)	93
Figure 4.17	DSC measurement of PET substrate (in N_2 ambient)	94
Figure 4.18	Procedures to perform surface texturing of PI substrate	96
Figure 4.19	Basic process flow of thin film Si solar cell fabrication on PI substrate	97
Figure 4.20	Configuration of thin film Si solar cells (a) based on p-n junction (b) based on p-i-n junction (figures not drawn to scale)	100
Figure 4.21	Metal mask used to define front Ag contact fingers (not drawn to scale)	105
Figure 4.22	Configuration of p-i-n junction thin film Si solar cell with white paint BSR incorporated below the PI substrate (figure not drawn to scale)	107
Figure 4.23	I-V curve of a standard solar cell under illumination	109
Figure 5.1	TGA plot of original PI and PET substrates (Original sample weight = 10 mg, heating rate = 20°C/min in N_2 ambient)	111
Figure 5.2	DSC plot of original PI substrate	113
Figure 5.3	DSC of original PET substrate	114
Figure 5.4	XRD pattern of original PI substrate	115
Figure 5.5	AFM image of original PI substrate (30 x 30 μm spot size)	116

Figure 5.6	Transmittance of PI (75 µm) in comparison to PET (250 µm) and glass (300 µm) substrates	117
Figure 5.7	Top view SEM images of textured PI substrates (10 kX magnification): (a) Original PI (b) Annealed at 400°C, 30 min (c) Annealed at 400°C, 60 min	118
Figure 5.8	AFM images of textured PI substrates (30 x 30 µm spot size): (a) Original PI (b) Annealed at 400°C, 30 min (c) Annealed at (b) 400°C, 60 min	119
Figure 5.9	Increase in surface roughness RMS after texturing process	120
Figure 5.10	EDX spectra of Al back contact (~1 µm) on textured PI substrate. Inset shows cross section diagram of Al on PI substrate (not drawn to scale)	122
Figure 5.11	AFM images Al back contact on textured PI substrate (30 x 30 µm spot size): (a) As-evaporated (b) Annealed at 400°C, 30 min	123
Figure 5.12	Sheet resistance of Al back contact on textured PI under different annealing temperatures (time fixed at 30 min, in N_2 ambient)	124
Figure 5.13	Surface reflectance of Al back contact on textured PI under different annealing temperatures (time fixed at 30 min, in N_2 ambient)	126
Figure 5.14	EDX spectra of Al-doped thin film Si on PI (Al/Si ratio = 5.95%). Inset shows cross section diagram of Al-doped Si on PI (not drawn to scale) and atomic percentage (at.%) of every element detected from the spectra	128
Figure 5.15	Raman spectra of Al-doped thin film Si subjected to different annealing durations (temperature fixed at 400°C, in N_2 ambient)	131
Figure 5.16	Raman spectra of c-Si substrate (reference sample)	132
Figure 5.17	Summary of Raman peak and FWHM under different annealing durations (temperature fixed at 400°C, in N_2 ambient)	133
Figure 5.18	Crystalline volume fraction (X_c) of Al-doped thin film Si under different annealing durations (temperature fixed at 400°C, in N_2 ambient)	134

Figure 5.19	XRD patterns of Al-doped thin film Si under different annealing durations (temperature fixed at 400°C, in N_2 ambient)	137
Figure 5.20	Top view SEM images of Al-doped thin film Si annealed under different durations (temperature fixed at 400°C, in N_2 ambient): (a) As-evaporated (b) Annealed at 400°C, 1 hour (c) Annealed at 400°C, 2 hours (d) Annealed at 400°C, 3 hours	140
Figure 5.21	AFM image of surface morphology of Si absorber layer after annealing at 400°C for 2 hours (Spot size 30 x 30 μm)	141
Figure 5.22	Resistivity of Al-doped thin film Si under different annealing durations (temperature fixed at 400°C, in N_2 ambient)	143
Figure 5.23	Hole concentration and hole mobility of p-type thin film Si under different annealing durations (temperature fixed at 400°C, in N_2 ambient)	144
Figure 5.24	Logarithmic plot of absorption coefficient of p-type thin film Si after annealing at 400°C for 2 hours	147
Figure 5.25	Plot of $(\alpha h\nu)^{1/2}$ as a function of photon energy (hv) of p-type thin film Si (annealed at 400°C for 2 hours)	149
Figure 5.26	Surface reflectance of p-type thin film Si (~1.5 μm) on flat and textured PI substrates	151
Figure 5.27	EDX spectra of intrinsic Si (~800 nm) on PI substrate. Inset shows cross section diagram of intrinsic Si on PI substrate (not drawn to scale)	152
Figure 5.28	Raman spectra of intrinsic Si (~800 nm) evaporated on p-type microcrystalline Si	153
Figure 5.29	Logarithmic plot of absorption coefficient of intrinsic Si evaporated on p-type microcrystalline Si	155
Figure 5.30	Plot of $(\alpha h\nu)^{1/2}$ as a function of photon energy (hv) of intrinsic Si evaporated on p-type microcrystalline Si layer	156
Figure 5.31	EDX spectra of Sb-doped thin film Si on PI (Sb/Si ratio = 8.07%). Inset shows cross section diagram of Sb-doped Si on PI (not drawn to scale) and atomic percentage (at.%) of Sb and Si detected from the spectra	157

Figure 5.32	AFM image of Sb-doped thin film Si emitter layer (30 x 30 μm spot size)	159
Figure 5.33	Surface reflectance of n-type thin film Si (~120 nm) evaporated on previous layers: p-type Si/Al/PI	161
Figure 5.34	XRD pattern of ZnO (~80 nm) window layer on PI. Inset shows cross section diagram of ZnO on PI substrate (not drawn to scale)	162
Figure 5.35	AFM image of ZnO window layer (30 x 30 μm spot size)	163
Figure 5.36	Transmittance of RF-sputtered ZnO (~80 nm) window layer on PI	165
Figure 5.37	Plot of $(\alpha hv)^2$ as a function of photon energy (hv) of RF-sputtered ZnO (80 nm) window layer on PI	167
Figure 5.38	Surface reflectance of thin film Si solar cells on PI substrates with and without ZnO (80 nm) anti-reflective coating (window layer)	168
Figure 5.39	A p-i-n thin film Si solar cell on PI substrate with ~80 nm ZnO ARC	169
Figure 5.40	Surface reflectance before and after introduction of white paint BSR (~1 μm thickness) at the back of the cell	170
Figure 5.41	Configuration of microcrystalline thin film Si solar cells fabricated on PI substrates: (a) Cell 1 (p-n + Al reflector + flat) (b) Cell 2 (p-n + Al reflector + textured) (c) Cell 3 (p-n + Al reflector + textured + ZnO) (d) Cell 4 (p-i-n + Al reflector + flat) (e) Cell 5 (p-i-n + Al reflector + textured) (f) Cell 6 (p-i-n + Al reflector + textured + ZnO) (g) Cell 7 (p-i-n + Al reflector + textured + ZnO + white paint BSR)	172
Figure 5.42	I-V characteristics of illuminated (AM 1.5, 220 W/m^2, 25°C) microcrystalline thin film Si solar cells (p-n junction) on PI substrates with various light trapping techniques	174
Figure 5.43	I_{sc} and V_{oc} of microcrystalline thin film Si solar cells with p-n junction. The right-most cell adopts the most light trapping strategies	176
Figure 5.44	I-V characteristics of illuminated (AM 1.5, 220 W/m^2, 25°C) microcrystalline thin film Si solar cells (p-i-n junction) on PI substrates with various light trapping techniques	177

Figure 5.45	Illuminated (AM 1.5, 220 W/m^2, 25°C) I-V and P-V characteristics of the best p-i-n thin film Si solar cell on PI substrate (η = 1.98%)	178
Figure 5.46	I_{sc} and V_{oc} of microcrystalline thin film Si solar cells with p-i-n junction. The right-most cell adopts the most light trapping strategies	179
Figure 5.47	Semi-logarithmic plots of dark I-V characteristics of p-n and p-i-n junctions microcrystalline thin film Si solar cells on PI substrates under forward-biased condition	181
Figure 5.48	Summary of efficiencies of microcrystalline thin film Si solar cells on PI substrates with p-n and p-i-n junction configurations. The right-most cells adopt the most light trapping schemes	185

LIST OF ABBREVIATIONS

AFM	Atomic force microscope
Ag	Silver
AIC	Aluminium-induced crystallisation
AIT	Aluminium-induced texturing
Al	Aluminium
AM	Air mass
Ar	Argon
ARC	Anti-reflective coating
As	Arsenic
ASTM	American Society for Testing and Materials
a-Si	Amorphous silicon
a.u.	Arbitrary unit
B_2H_6	Diborane gas
B	Boron
BSF	Back surface field
BSR	Back surface reflector
CB	Conduction band
CdTe	Cadmium telluride
CO_2	Carbon dioxide
c-Si	Monocrystalline silicon
Cu	Copper
CuO_2	Copper dioxide
CuInGaSe2/CIS	Copper indium gallium diselenide
CuInSe2/CIS	Copper indium diselenide
CVD	Chemical vapour deposition
CZ	Czochralski
DI	De-ionised
DSC	Differential scanning calorimetry
EDX	Energy dispersive X-ray
ELTRAN	Epitaxial layer transfer
EVA	Evaporated cells
F.F	Fill factor
FWHM	Full width at half maximum
FZ	Float Zone
GaAs	Gallium arsenide
GW	Gigawatt
H_2	Hydrogen
HNO_3	Nitric acid
HR-XRD	High resolution X-ray diffraction
HTS	High temperature substrate

HV	High vacuum
IB	Intermediate band
ICDD	International centre for diffraction data
In	Indium
InP	Indium phosphide
IPA	Isopropyl alcohol
IR	Infrared
ITO	Indium tin oxide
I-V	Current-Voltage
LTP	Layer transfer process
LTS	Low temperature substrate
mc-Si	Multicrystalline silicon
MG-Si	Metallurgical-grade silicon
Mo	Molybdenum
µc-Si	Microcrystalline silicon
µc-Si:H	Hydrogenated microcrystalline silicon
N_2	Nitrogen
Ni	Nickel
P	Phosphorus
pc-Si	Polycrystalline silicon
PECVD	Plasma enhanced chemical vapour deposition
PEN	Polyethylene naphthalate
PET	Polyethylene terephthalate
PH_3	Phosphine gas
PI	Polyimide
PSI	Porous silicon
Pt	Platinum
PV	Photovoltaics
PVD	Physical vapour deposition
QMS	Quasi-monocrystalline silicon
RE	Renewable energy
RF	Radio frequency
RMS	Root mean square
RTA	Rapid thermal annealing
Sb	Antimony
sccm	Standard Cubic Centimetres Per Minute
SCLIPS	Solar cells by liquid phase epitaxy over porous silicon
SCR	Space charge region
SeG-Si	Semiconductor-grade silicon
SEM	Scanning electron microscope
Si	Silicon
SiC	Silicon carbide
SiGe	Silicon-germanium
SiH_4	Silane
SIMOX	Separation by implantation of oxygen
SIMS	Secondary ion mass spectroscopy

Si_3N_4	Silicon nitride
SiO_2	Silicon dioxide
SoG-Si	Solar-grade silicon
SPC	Solid phase crystallised cells
SPS	Sintered porous silicon
SRH	Shockley Read Hall
SRV	Surface recombination velocity
STC	Standard test condition
Ta	Tantalum
TCO	Transparent conductive oxide
Te	Tellurium
TGA	Thermogravimetric analysis
TiO_2	Titanium dioxide
TIR	Total internal reflection
TO	Transverse optical
UHV	Ultra high vacuum
UMG-Si	Upgraded metallurgical-grade silicon
UNSW	University of New South Wales
USD	Dollar America
UV	Ultra violet
UV-Vis	Ultra violet-visible
VB	Valence band
VLSI	Very large scale integrated circuits
W	Tungsten
XRD	X-ray diffraction
ZMR	Zone melting re-crystallisation
ZnO	Zinc oxide

LIST OF SYMBOLS

α	Absorption coefficient
A	Cell area
B	Full width at half maximum (FWHM) of XRD pattern
c	Speed of light in vacuum
d	Thickness of ARC material
d	Crystallite size
D	Diffusion coefficient (diffusivity)
E	Electric field
E	Energy of photons
E	Illumination level
E_c	Energy of conduction band edge
E_f	Fermi energy or Fermi level
E_g	Optical band gap
E_{ph}	Energy of photon
E_v	Energy of valance band edge
f	Photon frequency
G	Generation rate of electron-hole pairs
h	Planck's constant
I	Current
I_a	Deconvoluted intensity of amorphous peak (in Raman)
I_c	Deconvoluted intensity of crystalline peak (in Raman)
I_L	Current source
I_0	Recombination current
I_{sc}	Short-circuit current
I_{max}	Maximum current
k	Crystal wavevector
k	Extinction coefficient
k	Boltzmann's constant
L	Carrier diffusion length
N	Photon flux
N_a	Acceptor concentration
N_d	Donor concentration
η	Power conversion efficiency
n	Ideality factor
n	Refractive index
Φ	Work function
Θ	Bragg angle of XRD pattern
Θ	Zenith angle (for AM calculation)
Θ_c	Critical angle at optical interface
P_{max}	Maximum power

q	Electronic charge
R	Reflectance
R	Resistance
R_s	Series resistance
R_{sh}	Shunt resistance
λ	Wavelength of light
t	Thickness of deposited film
T	Absolute temperature
T_c	Crystallisation temperature
T_g	Glass transition temperature
T_m	Melting temperature
τ	Carrier lifetime
v	Photon energy
V	Voltage
V_{oc}	Open-circuit voltage
V_{max}	Maximum voltage
W_{eff}	Effective cell thickness (cell volume/cell area)
X_c	Crystalline volume fraction
ΔH_f	Heat of fusion

SEL SURIA FILEM NIPIS SILIKON MELALUI KAEDAH PENYEJATAN TERMA ATAS BAHAN POLIMID

ABSTRAK

Teknologi konvensional yang berasaskan silikon (Si) wafer masih menguasai sekitar 90% pasaran photovoltaik (PV) dengan penukaran kecekapan sekitar 15 - 20% kerana wujudnya sumber silika yang banyak di dalam kerak bumi (~25%), tidak toksik di samping mempunyai jurang jalur yang hampir ideal (1.12 eV) untuk proses photoconversion. Tetapi, kos teknologi ini adalah tinggi (sekitar USD 2 - 3/$Watt_p$ pada masa ini) yang menghalangnya untuk digunakan secara meluas sebagai teknik alternatif untuk penjanaan kuasa pada masa ini. Ini berpunca daripada kos pemprosesan yang tinggi dan kos penulenan bahan Si (kos hablur tunggal adalah sekitar USD 400/kg) selain penggunaan bahan Si yang banyak (300 – 500 μm/wafer). Kajian ini mengupas potensi untuk menghasilkan sel suria Si filem nipis di atas permukaan substrat polimid (PI) kos rendah melalui kaedah penyejatan terma bagi mengurangkan kos teknologi ini di bawah USD 1/$Watt_p$. Sel suria direka dengan konfigurasi substrat berstruktur simpang p-n dan p-i-n. Pelbagai strategi memerangkap cahaya seperti pemantul aluminium (Al) sentuhan belakang, pentekstur permukaan PI, zink oksida (ZnO) salutan anti-pantulan (ARC) dan pemantul permukaan belakang (BSR) yang berasaskan cat putih telah dinilai untuk meningkatkan panjang jalan optik cahaya yang masuk dan untuk mengurangkan penyusutan foton akibat refleksi. Penyerap Si jenis-p berketebalan 1.5 μm telah digunakan dalam sel - sel simpang p-n manakala penyerap Si intrinsik berketebalan 800

nm telah digunakan dalam sel – sel simpang jenis p-i-n. Bilangan lohong dan elektron dalam Si jenis-p dan jenis-n (120 nm) adalah masing-masing bernilai 6.63 x 10^{18} cm^{-3} and 4.87 x 10^{19} cm^{-3} di kedua-dua jenis sel suria yang bersimpang p-n dan p-i-n, telah didopkan dengan Al dan antimoni (Sb) semasa penyejatan terma. Kedua-dua lapisan penyerap menunjukkan sifat mikrohablur selepas penyepuhlindapan selama 2 jam pada suhu 400°C dalam nitrogen (N_2) ambien dengan jurang jalur optik sekitar 1.0 – 1.2 eV. Sel – sel bersimpang p-i-n mencatatkan arus foto, faktor pengisian (F.F) dan kecekapan penukaran (η) yang lebih tinggi berbanding dengan sel – sel suria yang bersimpang p-n. Peningkatan strategi memerangkap cahaya dalam sel - sel menunjukkan peningkatan arus foto. Sel suria yang terbaik (dengan struktur simpang p-i-n) mempunyai V_{oc} 0.410 V, I_{sc} 8.00 mA, F.F 0.535 dan nilai η sebanyak 1.98%. Mekanisme – mekanisme utama yang mengurangkan kecekapan penukaran dikaitkan dengan kesan teduhan oleh sentuhan logam permukaan atas (14.1%), kelemahan penyerapan oleh Si filem nipis, penggabungan semula melalui Shockley Read Hall (SRH) di dalam bahagian tapak, pemancar dan simpang serta turut disumbangkan oleh kehilangan dalam pemancar yang disebabkan oleh isu jarak jari Ag.

THIN FILM SILICON SOLAR CELL PREPARED BY THERMAL EVAPORATION ON POLYIMIDE SUBSTRATE

ABSTRACT

Conventional wafer-based silicon (Si) technology still dominates around 90% of the photovoltaic (PV) market with 15 - 20% conversion efficiency due to its abundance (~25% of silica in the earth's crust), non-toxicity besides having close to ideal band gap (1.12 eV) for photoconversion process. But, this technology suffers from high cost/$Watt_p$ (USD 2 - 3/$Watt_p$ at present) that impedes its widespread to be an alternative power generation technique at present. This stems from high processing and purification costs of the Si material (single crystal costs about USD 400/kg) besides high material consumption (300 - 500 µm/wafer). This work explored the feasibility of fabricating thin film Si solar cells on low-cost polyimide (PI) substrates via thermal evaporation method in order to bring down the costs of the Si PV technology to below USD 1/$Watt_p$. The solar cells were fabricated in substrate-configuration with p-n and p-i-n junction structures. Various light trapping strategies such as aluminium (Al) back contact reflector, PI surface texturing, zinc oxide (ZnO) anti-reflective coating (ARC) and white paint back surface reflector (BSR) have been evaluated to increase optical path length of the incident light and to reduce reflection losses. A 1.5 µm thick p-type Si absorber was used in the p-n junction cells while 800 nm intrinsic Si was adopted in the p-i-n junction cells. The hole and electron concentrations in the p-type and n-type Si (120 nm) were respectively 6.63 x 10^{18} cm^{-3} and 4.87 x 10^{19} cm^{-3} in both p-n and p-i-n junction cells,

realised by doping with Al and antimony (Sb) during the evaporation. Both absorber layers showed microcrystalline nature after 2 hours of annealing at 400°C in nitrogen (N_2) ambient with optical band gap (E_g) of around 1.0 – 1.2 eV. The p-i-n junction cells recorded higher photocurrent, fill factor (F.F) and conversion efficiencies (η) compared to the p-n junction counterparts. Increased light trapping strategies in the cells showed increased photocurrent. The best cell (with p-i-n junction structure) measured V_{oc} (open-circuit voltage) of 0.410 V, I_{sc} (short-circuit current) of 8.00 mA, F.F of 0.535 and η of 1.98%. The main loss mechanisms were associated to contact shading loss (14.1%), poor absorption of the Si thin film, Shockley Read Hall (SRH) recombination in the base, emitter and junction regions and also contributed by emitter losses due to silver (Ag) finger spacing issues.

CHAPTER 1

INTRODUCTION

1.1 Solar Energy

Today, the world's population has witnessed how bad the effect of climate change could be by tragedies that hit the entire cities in New Orleans (2005) and temperatures up to 50°C that hurt people and ecosystem in southern Europe in the summer 2007. These tragedies has sent out a signal that carbon dioxide (CO_2) emissions need to be curbed very soon and a promising renewable energy (RE) source like solar energy has to be deployed in a massive scale in order to combat the climate change (EPIA, 2010). The need for the solar energy is amplified further by the enormous fluctuations of oil prices in the last few years that stem from the volatility of the financial markets besides economic turmoil which have highlighted our strong dependence on oil. Apart from that, the latest nuclear tragedy in Japan has brought some countries to revise their future energy plans (IEA, 2010).

Figure 1.1: Monocrystalline silicon (c-Si) solar panel.

The solar energy is a RE that can be harvested from the sun's rays by using photovoltaics (PV) technology (as shown by Figure 1.1). The PV technology (i.e. solar panel formed by an array of solar cells) normally comprise of a semiconductor material (such as silicon, Si) that can absorb the incoming photons (from sunlight) and convert them into useful electric current via a mechanism called "photovoltaic effect" (Green, 2002b).

Electricity generation via the PV technology is now the fastest-growing business (Razykov et al., 2011, Parida et al., 2011). The cumulative worldwide annual PV installed capacity is doubling every 2 years as observed from Figure 1.2. The PV market has grown at a rate of 40% each year, with cumulative worldwide installed capacity of around 15 GW_p in 2008 (EPIA, 2010).

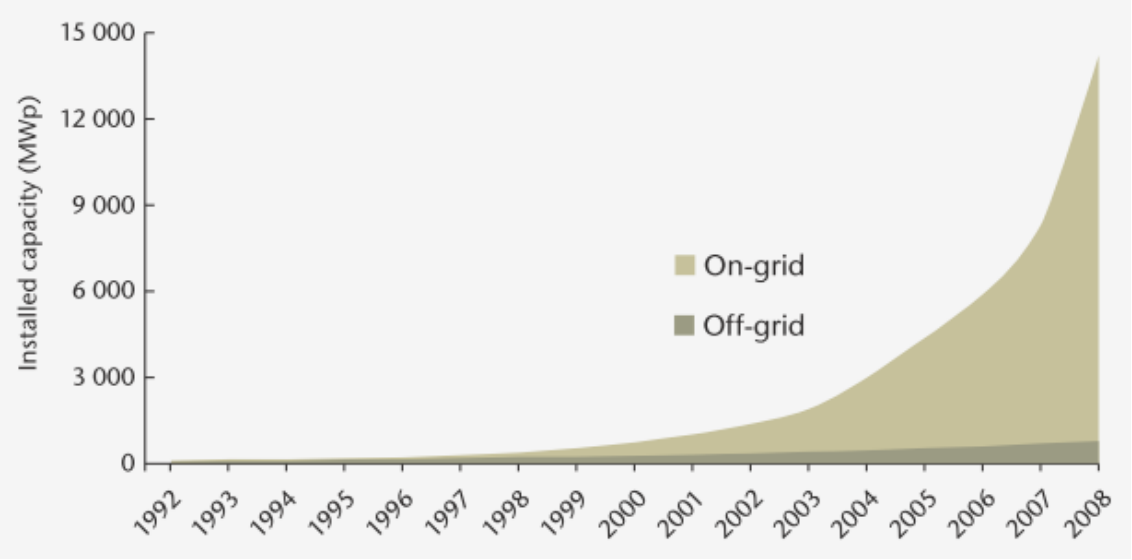

Figure 1.2: Cumulative worldwide annual PV installed capacity (EPIA, 2010).

If compared to other REs, the PV technology is more favourable due to several factors. First, it exploits the most abundant and inexhaustible source of free power from the sun unlike other sources of energy (Parida et al., 2011). Besides, the PV technology has a higher energy density (i.e. energy delivered over the lifetime of a device per unit mass of material) compared to most other energy technologies. Coal, biomass and natural gas exhibit around 30 – 50 MJ/kg. The PV technology (200 μm, Si-based with 15% efficiency and 20 years lifetime) shows around 10^4 – 10^5 MJ/kg while a nuclear energy normally has a much higher energy density of around 10^6 MJ/kg (Bowden et al., 2010).

Apart from that, the PV technology can be deployed almost anywhere with sunshine. The system is easy to install and involve low maintenance. It also has negligible environmental footprint. During operation, the PV technology produces electricity with no air emissions and no waste production. Furthermore, there is no CO_2 emission, thus has a very low carbon footprint suitable to combat the climate change. This technology is also modular, in the sense that it ranges from milliwatt (mW) in consumers products up to gigawatt (GW) in future power stations. On top of that, the PV technology is also robust and reliable with proven lifetime of 20 – 30 years (IEA, 2010, Green, 1982). The PV technology on Si platform utilises existing technologies and manufacturing processes in microelectronics, making it cheap and efficient to implement.

However, the most prominent drawback of the PV technology (particularly wafer-based Si) is due to its high cost/$Watt_p$ (around USD 2 - 3/$Watt_p$ at present) of the finished module compared to USD 1/$Watt_p$ of coal-electricity generated source

(Aberle, 2000). This is the main reason that hampers the widespread adoption of the PV technology to be the alternative source of power generation.

1.2 Efficiency and Cost Projections of Solar Technologies

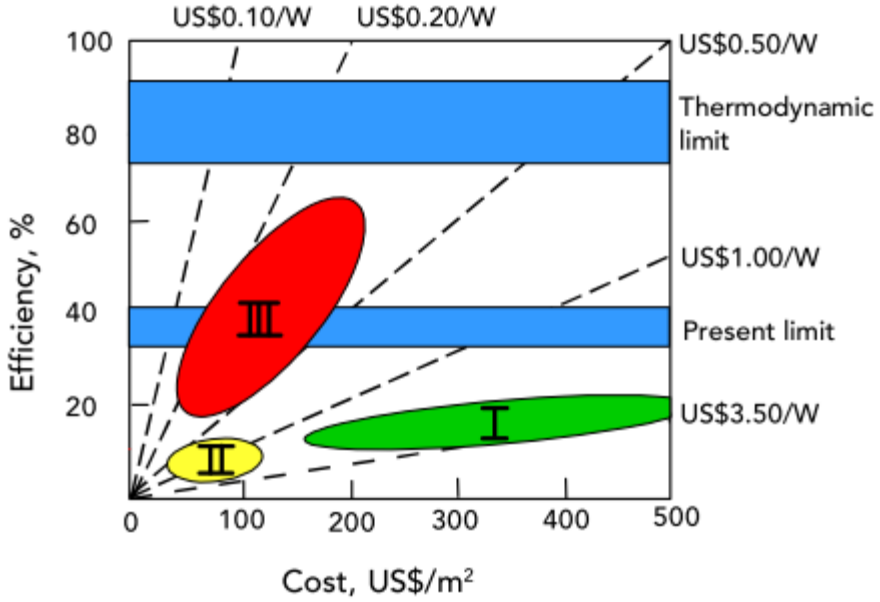

Figure 1.3: Efficiency and cost projections of three generations of solar technologies (First generation: wafers, Second generation: thin films, Third generation: advanced thin films) (Green, 2003).

Figure 1.3 shows the efficiency and cost projections of three different generations of solar technologies categorised by the ARC Photovoltaics Centre of Excellence, UNSW, Australia (Green, 2003). The figure plots efficiency against manufacturing costs of each generation (in USD/m^2).

The first generation consists of monocrystalline (c-Si) and multicrystalline (mc-Si) wafer-based Si solar cells. This generation possesses high efficiency (10 – 20%) with relatively high production costs. This is due to high energy and material-intensive

Czochralski (CZ), Float Zone (FZ) and casting/directional solidification processes used to produce both high purity c-Si and mc-Si wafers respectively (Mahajan and Harsha, 1999). The present manufacturing costs of this generation is as low as USD 2 – 3/$Watt_p$ (for large scale manufacturers). USD 1/$Watt_p$ will likely be the bottom limit of the costs for this generation if the conversion efficiency can be increased or the costs can be reduced (Green, 2003).

The second generation is the thin film technology typically deposited on foreign substrates or superstrates, usually glass or plastic. This technology involves several device families such as amorphous Si (a-Si), polycrystalline Si (pc-Si), microcrystalline Si (µc-Si), cadmium telluride (CdTe), copper indium diselenide ($CuInSe_2$, CIS) and also copper indium gallium diselenide ($CuInGaSe_2$, CIGS). Out of these, Si-based thin films are more superior in terms of stability, manufacturability, toxicity (related to Cd) and resource availability (related to Te and In) issues (Green, 2009). With regard to Si thin films in this generation, focus is given on depositing the thin films by evaporation rather than chemical vapour deposition (CVD) related processes. Evaporation is preferable due to its simplicity and avoidance of dangerous gas like silane (SiH_4) that is typically used for Si deposition in a CVD system. The solar cells of this generation have a much lower manufacturing costs/area since the glass and plastic substrates are way cheaper than the wafers. But, the conversion efficiency only shows around 5 – 15%. However, the lower efficiency trades-off the overall costs to be 2 - 3 times lower than that of the cells from the first generation (Green, 2003).

The third generation are highly efficient thin film cells which lie on advanced concepts of PV (advanced thin films). The manufacturing costs of this generation are

equal to the costs of the second generation since they are both based on thin film deposition techniques (i.e. cheaper than wafer-based). The distinct difference of this generation is that the cells are not constrained by the same efficiency limit of the first and second generations (31% efficiency under non-concentrated sunlight) (Green, 1994). The efficiency limit of this generation is 74% (Farrell and Ekins-Daukes, 2011) under non-concentrated sunlight thereby lowering the final costs of the cells of this generation to 2 to 3 times lower than that of the second generation cells. The examples of research areas being conducted by UNSW in this respect are on all Si tandem cells based on band gap engineering of Si nanostructures in amorphous matrix (oxides, nitrides and carbides), photon up and down-conversion (via spectral modification) and hot carrier effects in solar cells (Conibeer et al., 2006, König et al., 2010).

1.3 Problem Statement

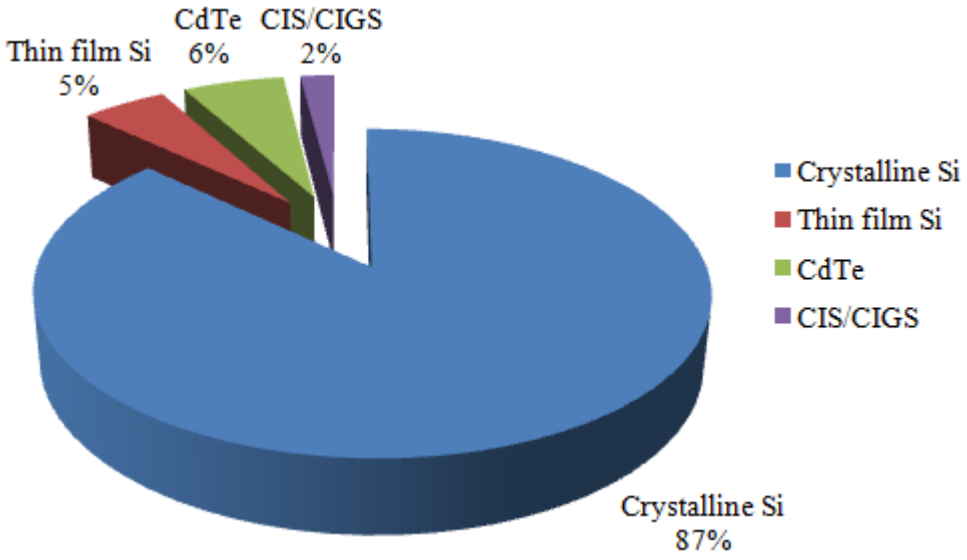

Figure 1.4: PV market shares in 2010 (breakdown by technology) (EPIA, 2010).

Si is still the material of choice to fabricate solar cells due to its abundance (about 25% of silica in the earth's crust), non-toxicity, proven product durability, good electronic properties and extensive knowledge on the existing microelectronics technologies (Green, 2000). Besides, Si has a band gap (1.12 eV) that is close to the band gap of an ideal photoconverter (1.4 eV) (Nelson, 2003). Due to these facts, Si in its conventional crystalline technology (wafer-based composed of c-Si, mc-Si and ribbon c-Si) still dominates around 87% of the PV market with stable efficiency of around 10 - 20% (shown by Figure 1.4). This domination is expected to continue for at least the next 10 years (Beaucarne, 2004).

The main setback of the wafer-based Si technology is its high cost. The c-Si of semiconductor-grade (SeG-Si) with high purity (impurity concentration < 1 ppb) and crystal perfection produced by Czochralski (CZ) and Float-Zone (FZ) techniques proves to yield highly efficient Si solar cells but these growth techniques are highly energy-intensive due to necessity of multiple purification steps. This makes the final c-Si very expensive (high purity c-Si is priced at around USD 400/kg). On the other hand, the semiconductor grade mc-Si produced via casting and directional solidification techniques involves lower capital costs, higher throughput and also shows higher tolerance to poor feedstock quality with respect to the c-Si. The mc-Si is sold at around USD 80/kg and the mc-Si cells normally have 80% of the performance of the c-Si cells made on CZ wafers (Ceccaroli and Lohne, 2005, Pizzini, 1982).

Besides being highly energy-intensive, both types of wafers are also highly material-intensive since the thickness of the Si wafer is made to be in the order of hundreds of microns, typically 250 - 300 μm, in order to ensure a complete absorption

of the incident sunlight, owing to the fact that Si is an indirect band gap semiconductor material with poor absorption capability (Runyan, 1965). Besides, the cost of the Si material alone makes up around 50% of the total costs of a finished PV module (Rubin, 2010). These factors ultimately lead to a high cost/$Watt_p$ of the wafer-based Si solar cells in the market, typically as low as USD 2 - 3/$Watt_p$ (for large scale manufacturers) (Green, 2003), impeding its widespread to be an alternative power generation technique at present.

1.4 Scope of Research

Having reviewed Section 1.2 and 1.3 above, this work will explore the second generation thin film Si solar cell technology (as in Figure 1.3) deposited on foreign substrates via thermal evaporation method as a way to reduce the cost/$Watt_p$ of the final solar cells (due to lower material consumption).

The Si thickness will be around 1 - 2 μm to reduce the material consumption (150 times Si thickness reduction compared to the conventional wafers) (Green, 1994). The poor photons absorption at such a low absorber thickness is going to be compensated with several light trapping techniques. The substrate will be a low-cost plastic material (polymer) since it is much cheaper compared to the Si wafers. Besides, the plastic substrate is also attractive since it is light in weight, highly flexible, unbreakable, portable to consumers besides being capable of roll-to-roll deposition process (Rath et al., 2008). Thermal evaporation is chosen to be the deposition method since it requires only a simple setup besides being easy to operate (Chopra, 1969).

Combined low Si material consumption and low-cost plastic substrate could potentially lead to low-cost thin film Si solar cells (i.e. low cost/$Watt_p$) if reasonable device conversion efficiency can be realised.

1.5 Objectives of Research

The objectives of this work are as follows:

1. To fabricate and characterise thin film Si solar cells on polyimide (PI) substrates via thermal evaporation
2. To study the effect of light trapping schemes on I_{sc} and V_{oc} of thin film Si solar cells
3. To investigate the performance and identify loss mechanisms of p-n and p-i-n cells

This work does not aim to produce high efficiency thin film Si solar cells on the PI substrates, but rather to understand the underlying mechanisms that govern the performance of the solar cells.

1.6 Organisation of Thesis

Chapter 1 explains the solar energy, efficiency and cost projections of solar PV technologies and problem statement. The scope and objectives of this research are also outlined in this chapter.

Chapter 2 deals with a brief literature review of solar cell device families, strategies towards cost reduction and progress in thin film Si solar cells research and development activities.

Chapter 3 presents the basic physics and relevant theories to the thin film Si solar cells such as photovoltaic effect, the solar spectrum, thermal evaporation process, thin film Si solar cells physics and finally related loss mechanisms.

Chapter 4 covers the materials and methods involved in the fabrication of thin film Si solar cells on PI substrates in this work. These include the deposition and characterisation equipments in use to fabricate and investigate the structural, surface morphology, optical and electrical properties of the deposited layers. Besides, this chapter also includes the detailed process flow to fabricate the thin film Si solar cells on PI substrates.

Chapter 5 presents the experimental observations, calculations and explanations of the findings. They span from the results of every characterised layer until the performance of the final solar cells.

Chapter 6 concludes the overall findings and gives recommendations for future works on the fabrication of thin film Si solar cells on PI substrates.

CHAPTER 2

LITERATURE REVIEW

2.1 Solar Cell Device Families

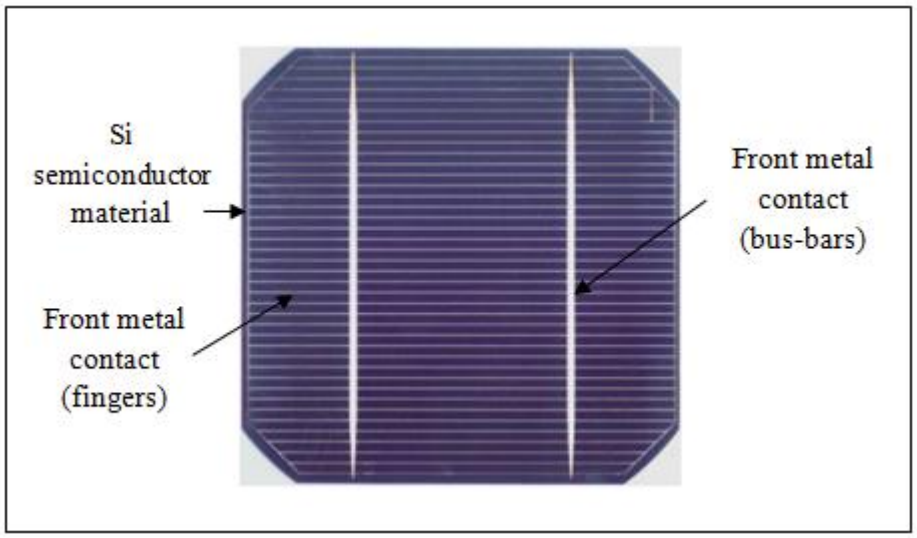

Figure 2.1: Monocrystalline (c-Si) solar cell.

In general, solar cells can be classified into a few categories (or called generations) as previously discussed by Figure 1.3. The first generation is the crystalline Si (wafer-based) solar cells (as shown in Figure 2.1). The Si material has an optical band gap (E_g) of 1.12 eV at room temperature (300 K). The first generation cells comprise of c-Si and mc-Si with thicknesses of 300 – 500 μm. These cells are characterised by high optical absorption, high minority carrier diffusion lengths, high conversion efficiencies (10 – 20%) with relatively high production costs (USD 2 - 3/$Watt_p$) (Green, 2003).

The second generation solar cells comprises of thin film technologies such as CdTe (E_g = 1.44 eV), CIGS (E_g ranges from 1.02 to 1.65 eV depending on gallium content), a-Si (E_g = 1.8 eV), μc-Si (E_g = 1.12 eV), pc-Si (E_g = 1.12 eV) and polymer-based solar cells (Shah et al., 2004). The thin film solar cells are typically deposited via chemical vapour deposition (CVD), physical vapour deposition (PVD), electrochemical and spin-on methods on foreign substrates like glasses, stainless steels and also on flexible plastic materials. The foreign substrates help to retain the mechanical strengths besides avoiding the breakage of the films. The thin film solar cells possess fairly high optical absorption (especially for CdTe and CIGS), low minority carrier diffusion lengths (due to the presence of defects and grain boundaries), low conversion efficiencies (5 – 15%) but with two to three times lower production costs compared to the first generation cells (Nelson, 2003). These cells are normally designed with light trapping properties to increase optical path length of the incident sunlight and hence photogeneration (Brendel, 2005a).

The third generation solar cells are designed based on advanced concepts of PV (advanced thin films) (Green, 2003). While the thermodynamic limit (so-called Landsberg's limit) of power conversion is around 93% (illustrated in Figure 2.2) (Farrell and Ekins-Daukes, 2011), the third generation cells have 74% efficiency limit under non-concentrated sunlight (compared to 31% for the first and second generation cells under non-concentrated sunlight as defined by Shockley and Queisser via the principle of detailed balance (Shockley and Queisser, 1961)).

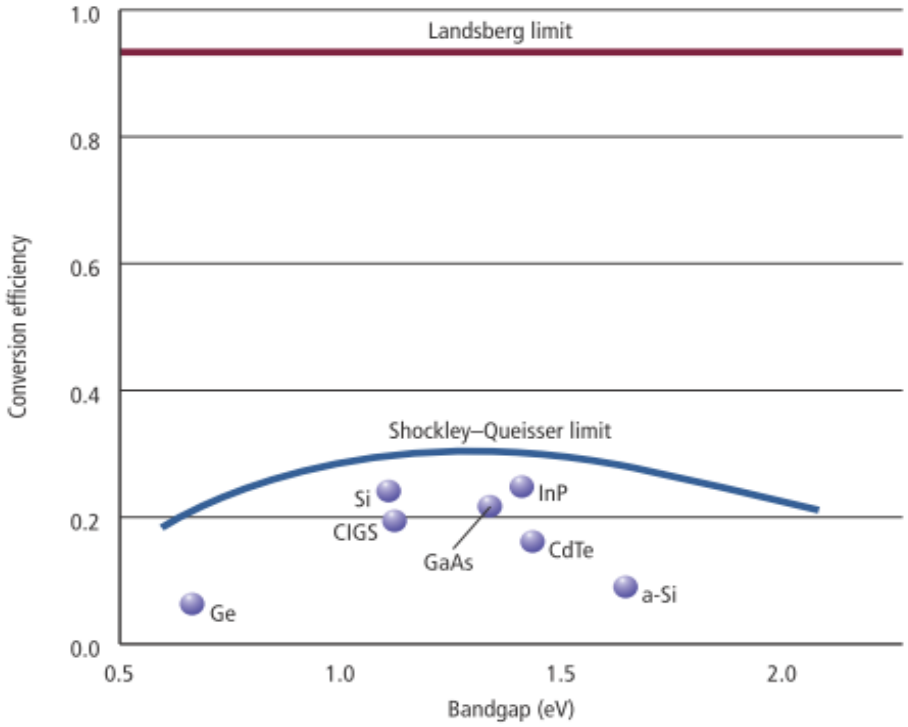

Figure 2.2: The ultimate efficiency limit of solar energy conversion (Landsberg's limit) (Farrell and Ekins-Daukes, 2011).

The third generation cells can be deposited by the same methods employed to produce the second generation cells thus holding a big potential of reducing the overall PV module costs (since higher conversion efficiencies can be attained). Research and developments are being heavily carried out worldwide on multi-junction cell structures, nanostructures and quantum dots, hot carrier cells, intermediate band (IB) cells, up and down-conversion cells (via spectral modification), multiple excitons generation cells and also on concentrator PVs (Conibeer et al., 2008, Conibeer et al., 2006, Hao et al., 2009, König et al., 2010, Green, 2002c, Tang and Sargent, 2011).

2.2 Strategies Towards Cost Reduction

In order to be competitive with fossil fuel or nuclear power generation, the cost of PV energy has to be reduced tremendously. With regard to Si technology, the cost of Si alone already accounts for about 50% of the production costs of current industrial wafer-based solar cells (Aberle, 2006b). In order to reduce the amount of consumed Si, the PV industry is counting on a number of options that are now being developed in research. One of the options is to use a lower quality Si, called metallurgical-grade Si (MG-Si) with 98% purity (impurity concentration ~ 500 ppm) or upgraded metallurgical-grade Si (UMG-Si) with higher quality than the MG-Si. Besides, solar-grade Si (SoG-Si) can also be used (impurity concentration ~ 10 – 50 ppm) as a replacement (Ceccaroli and Lohne, 2011).

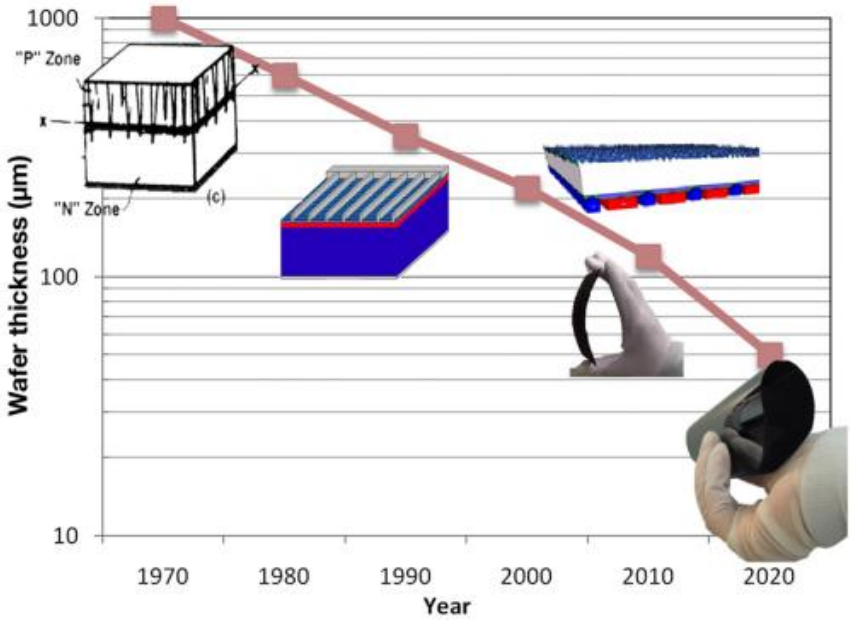

Figure 2.3: Reduction of substrate (absorber layer) thickness as a potential solution for cost reduction (Bowden et al., 2010).

Having known the fact that the Si material costs 50% of the overall production costs of a PV module, one solution to reduce the costs is by going for thin film Si solar cells (as shown in Figure 2.3), typically in the order of less than 5 μm (Poortmans, 2006). The solar cells are normally deposited on foreign substrates (like glass, plastic, stainless steel, ceramic) to provide mechanical strength (R. Catchpole et al., 2001). However, the major drawback of the thin film Si solar cells is its relatively low conversion efficiency due to weak optical absorption at low thickness (Green, 1995). This issue will be elaborated further in the next section.

2.3 Progress in Thin Film Silicon Solar Cells Research

Thin film Si solar cells have been making substantial progress through decades of research and development activities. The driving force is to reduce the amount of the expensive crystalline Si consumed by the 300 μm wafer-based Si solar cells (Green, 2001). PV community agreed that for the cell to be considered thin, the effective thickness (W_{eff} = cell volume/cell area) should be below 50 μm. However, device thickness of below 10 μm is typically chosen to indicate a clear margin in the Si saving (Brendel, 2005b).

2.3.1 Issues of Thin Film Silicon Solar Cells

The reduction of Si thickness to below 10 μm in a thin film Si solar cell can suppress the costs of PV modules tremendously. However, at this thickness level, the physical limit of power conversion becomes a question. The limitation is imposed by several issues that need to be tackled before high efficiency cells can be realised.

The most fundamental issue is Si absorbs poorly at low thickness. At the thickness of 1 – 10 μm, the near infrared (IR) fraction of the incident sunlight is hardly absorbed since Si has a low absorption coefficient (α) in this region. This is worsened by the fact that Si is an indirect band gap semiconductor (Brendel, 2005a). To mitigate the poor absorption, light trapping strategies are incorporated within the thin film Si solar cells. The purpose is to increase the optical path length of the light within the cells via multiple internal reflections. Higher optical path length leads to higher potential of photons absorption (i.e. cell has high optical thickness) and hence higher photocurrent (Cho et al., 2011b). The incident light can be trapped more effectively in the device by incorporating anti-reflective coating (ARC) on top of the device (typically silicon dioxide (SiO_2), silicon nitride (Si_3N_4), zinc oxide (ZnO), indium tin oxide (ITO) or titanium dioxide (TiO_2)) (Müller et al., 2004, Yang et al., 2011), surface texturing (through natural surface morphology during deposition, laser etching, plasma etching or thin film etch back), substrate texturing (laser etching, sandblasting, plasma etching) (Vazsonyi et al., 1999), back contact reflector (uses metal, dielectric or multi-layer porous) (Sai et al., 2009) or by using silver (Ag) plasmonics nanostructures (Pillai and Green, 2010, Zhu et al., 2010).

Recombination at defects is another issue that needs to be addressed. In a typical thin film Si solar cell, defects are generated through incorporation of impurities into the Si host atoms during doping and structural imperfections during thin film deposition (growth). Defects appear in the forms of lattice mismatch, grain boundaries and dangling bonds and lead to the formation of extra states within the band gap that act as effective trap states and recombination centres to electron-hole pairs (Mahajan and

Harsha, 1999). This problem can be tackled by depositing the thin film Si layer in a high temperature deposition process (or low deposition temperature but high successive annealing temperature) to produce large grains absorber as well as for in-situ defect annealing (Rau et al., 2009). But, this hinders the usage of foreign substrates like glass and plastic where high deposition temperature is not feasible due to thermal stability of the substrates. The dangling bonds within the film can be saturated via passivation by hydrogen (H_2) gas (Honda et al., 2006). At the same time, the surface of the thin film (front and rear) can be passivated by either silicon dioxide (SiO_2) or silicon nitride (Si_3N_4) in order to reduce carrier surface recombination velocity (hence surface recombination rate) (Aberle, 2000).

2.3.2 Methods and Approaches

Several techniques have been investigated by PV researchers around the world in order to reduce the costs of crystalline Si solar cells. Generally, these techniques can be classified into 3 main groups depending on types of substrates being used for deposition of the Si layers; cells from thinned monocrystalline Si (c-Si) wafers, cells fabricated on high temperature substrates (HTS) and cells fabricated on low temperature substrates (LTS) (Brendel, 2005b).

The first method thins down the original CZ and FZ c-Si substrates before the device fabrication. The feasibility of high cell efficiency with thin crystalline Si layers was demonstrated experimentally with a confirmed device efficiency of 20.6% by Brendel et al. and 21.5% by Zhao and co-workers. Both cells were 47 μm thick and fabricated from thinned FZ wafers (Kim et al., 2006). Hebling et al. succeeded in

fabricating a 19%-efficient cell 49 μm in thickness grown by chemical vapor deposition (CVD) on a SIMOX (separation by implantation of oxygen) wafer. The cell has both front and back contacts (Hebling et al., 1997). However, all the above cells were processed using five or more photolithography steps, therefore not cost-effective.

Layer transfer process (LTP) is another approach employed to fabricate lower cost solar cells on c-Si substrates. This technique uses a special surface conditioning of the substrate (reusable) that allows the transfer of the device layer to a low-cost device carrier (like plastic or glass materials). Using a c-Si wafer as a growth substrate enables fabrication of c-Si cells by homo-epitaxial process (Bergmann et al., 2002). In LTP, the most common surface conditioning technique being used is via formation of porous Si layer. This includes techniques like epitaxial layer transfer (ELTRAN), sintered porous Si (SPS), porous Si (PSI), quasi-monocrystalline Si (QMS) and solar cells by liquid phase epitaxy over porous Si (SCLIPS) (Brendel, 2005b).

Thin film Si solar cells on HTS are typically fabricated at temperatures above 800^{o}C on substrates such as low-quality Si (i.e. MG-Si), graphite, ceramics, high temperature glass, Si carbide (SiC) and also on ribbon Si (Slaoui et al., 2002, Solanki et al., 2002). Using this technique, conversion efficiency as high as 18% can be realised. Bai et al. declared thin film Si solar cell with 16.6% efficiency on high temperature-resistance substrates (details not disclosed) with minority carrier diffusion length of over 150 μm after implementing impurity gettering and hydrogen passivation to the as-grown Si (Bergmann and Werner, 2002). Some research groups have been working on zone melting re-crystallisation (ZMR) technique where Si is crystallised at its melting point (T_{melt} ~ 1400 ^{o}C) in order to get as large grain as possible. In these

works, ceramics, graphite and oxidised Si wafers have been used as substrates involving 30 - 100 µm of Si thickness (Reber et al., 2001). Mitsubishi Corporation reported a conversion efficiency of 16.5% for an epitaxial Si film deposited on a ZMR Si film (on oxidized Si wafers). With the same process, Fraunhofer ISE declared 9.3% conversion efficiencies for cells on ceramics and 11% for cells fabricated on graphite. ASE Corporation announced 8.3% efficiency for a cell on fabricated on graphite via the same technique (Bergmann, 1999).

Besides ZMR, plasma spray is another high temperature process used to deposit thin film Si on high temperature-resistance substrates. Daido Hoxan and Tonen Corporation reported 10.7% conversion efficiency using 500 µm Si and 4.3% on 330 µm of Si. As for cells produced by electrodeposition process, Global Photovoltaics Incorporation reported 8.0 – 8.4% efficiency for 50 µm of Si thin film on polyester, ceramics and clay tile (Bergmann, 1999).

Figure 2.4: PECVD system.

Cells on LTS are fabricated with deposition temperatures up to 550^{o}C on low-cost substrates like glass, metal foil and plastic (Yamamoto et al., 2000). At low deposition temperatures, the interaction of the substrates with the active devices can be kept small. Thus, the out-gassing and out-diffusion of contaminants from the substrates into the devices is reduced in comparison to the high temperature deposition techniques (Brendel, 2005b). In the literature, a lot of research and development activities pertaining thin film Si solar cells on the LTS have been carried out (or still in progress) on glass substrates (Aberle et al., 2001, Brinza et al., 2009). The University of New South Wales (UNSW, Sydney) is one institution that is now heavily researching thin film Si solar cells on the glass substrates. The main area of research includes SPC (solid phase crystallisation) cells, EVA (evaporated) cells and hybrid cells that are made in combination of SPC and EVA techniques (Aberle, 2006b).

The SPC cells are made of 2 µm thick a-Si precursor deposited by 13.56 MHz PECVD system (as shown in Figure 2.4) on 3.3 mm thick borosilicate glass (Schott Borofloat33) in superstrate configuration (where the glass faces the incident sunlight). The fabrication starts with surface texturing of the glass via aluminium-induced texturing technique (AIT) (Aberle et al., 2006) to produce surface with roughness root mean square (RMS) of around 60 – 150 nm. The purpose is to reduce reflection losses and for efficient light trapping. A 75 nm of Si_3N_4 (refractive index, n ~ 2.1 at 633 nm) anti-reflective coating (ARC) is then PECVD-deposited on the textured glass to help reduce the reflection further besides trapping more of the incident sunlight. The a-Si precursor (with 2 µm p-type Si absorber with doping level of 1 x 10^{16} cm^{-3}, 100 nm n-type emitter with doping level of 5 x 10^{19} cm^{-3}) is then deposited by PECVD

(deposition rate~ 30 nm/min) and crystallised at 600^{o}C for 24 hours to high quality pc-Si via SPC process. The cells are then annealed (via rapid thermal annealing, RTA) to activate dopants (1000^{o}C, 1 min) and followed by hydrogenation (600^{o}C, 30 min) to passivate defects within the film. Metallisation is done by applying a back surface field (BSF) layer before evaporation of photolithographically-defined 1 μm-thick inter-digitated contacts on the rear surface of the cells. This technology has been commercialised by CSG Solar AG with modules conversion efficiency of 7 – 8% (with open-circuit voltage, V_{oc} ~ 0.450 to 0.500 V, fill factor, F.F ~ 0.698) in Thalheim (Germany) since 2006 (Aberle, 2006a).

The EVA cells (collaboration of UNSW and CSG Solar) are produced via e-beam evaporation process with motivations to get rid of toxic gases (such as SiH_4 precursor used for Si deposition in PECVD system for SPC cells) besides the simplicity and attractively high deposition rate of the e-beam system (around ~1 μm/min). Apart from that, the e-beam deposition can be performed in a non-ultra high vacuum (UHV) environment (base pressure > 10^{-8} Torr, deposition pressure > 10^{-7} Torr). Thus, the thin film Si deposition via the e-beam evaporation system is a relatively cost-effective approach (Kunz et al., 2009a).

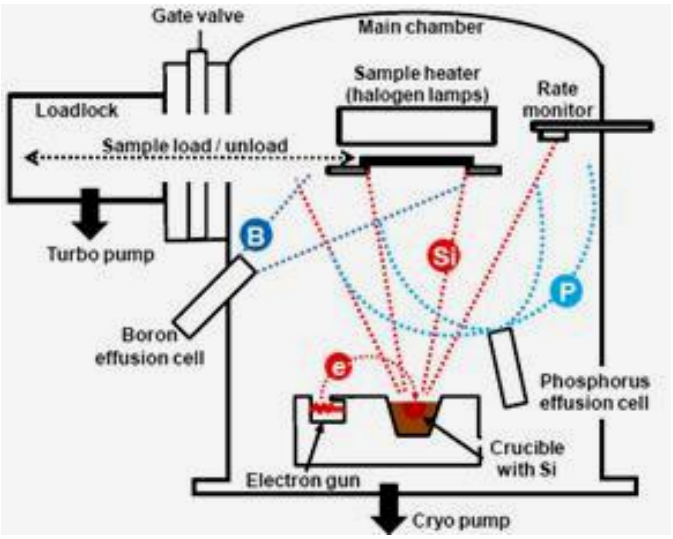

Figure 2.5: Schematic the of Si e-beam evaporation system with boron and phosphorus effusion cells for in-situ doping used in UNSW (UNSW, 2009).

The pc-Si EVA cells are prepared in the same configuration as the SPC cells (also on 3.3 mm Schott Borofloat33 glass). All other process steps and parameters remain the same. The thin film Si deposition is carried out on the e-beam evaporation system equipped with boron and phosphorus effusion cells for in-situ doping of Si (as illustrated in Figure 2.5). For the EVA cells, the glass substrates are not textured to prevent the development of microcracks and voids in the film after RTA step since the deposited Si on textured glass is of low density (Kunz et al., 2009a). The formation of defects within the cells leads to shunting problem and causes low V_{oc} values during current-voltage (I-V) measurements (Kunz et al., 2009b).

Since the glass substrates cannot be textured, other light trapping strategies have been explored and incorporated to the EVA cells. One of the light trapping features exploited is via a highly reflective white paint back surface reflector (BSR) painted by a low-cost spray technique at the rear side of the cells. The purpose of this layer is to collect all the transmitted light which would otherwise be lost (Berger et al., 2007).

Besides, Si etch-back texturing process has been applied to the cells via chemical and plasma etching techniques. With these improvements, a new UNSW efficiency record of 7.1% (V_{oc} ~ 0.458 V, J_{sc} ~ 26.6 mA/cm^2, F.F ~ 0.58) has been demonstrated on the EVA cells. The J_{sc} of 26.6 mA/cm^2 is the highest current density ever reported from thin film evaporated pc-Si solar cells (UNSW, 2011). Apart from the above cells, hybrid cells have also been evaluated by UNSW. The hybrid cells that combine PECVD emitter with evaporated BSF and absorber layer can be annealed at 640^{o}C for only 2 hours via the SPC technique and capable to deliver comparable I-V performance as the normal SPC cells (conversion efficiency of 7 – 8%) (UNSW, 2009).

Development works on thin film Si solar cells on plastic substrates such as polyimide (PI), polyethylene terephthalate (PET) and polyethylene naphthalate (PEN) are still fairly new (Mase et al., 2002, Rath et al., 2008). Despite being low-cost, light-weight, portable and capable for inline roll-to-roll deposition process, low glass temperature (T_g) of the plastic substrates render them unstable during high temperature (or long duration) processing or annealing. This is why the deposition of Si thin film on the plastic substrates is normally carried out at temperatures below 200^{o}C (Brendel, 2005b). When the processing and annealing steps are limited to below this temperature, the main challenge is to crystallise the Si thin film to high crystal quality without deforming the substrates.

Hydrogenated thin film microcrystalline Si (μc-Si:H) solar cells with p-i-n structure (μc-Si:H intrinsic layer) on plastic substrates with efficiencies of 9.4% and 5.9% at PECVD deposition temperatures of 140^{o}C and 100^{o}C respectively have been demonstrated by Kondo et al. (Kondo et al., 2002). Another work of μc-Si:H solar cells

with n-i-p structure (μc-Si:H intrinsic layer) deposited on plastic substrates with conversion efficiency of 5.5% (F.F = 0.525, V_{oc} = 0.920 V, J_{sc} = 11.6 mA/cm^2) at hot wire-CVD (HWCVD) deposition temperature of 150^{o}C has been demonstrated by Filonovich et al. (Filonovich et al., 2008).

Works of thin film Si solar cells via thermal evaporation system are hardly reported in the literature. One of the reasons is due to its relatively inferior film quality (such as conformality, step coverage, uniformity) produced the highly directional deposition nature if compared to the most commonly used CVD techniques (Runyan, 1965, Aberle, 2006b) that are highly multi-directional during the deposition. This results in a better film conformality, step coverage and uniformity across the substrates. However, the development activities of EVA cells (e-beam evaporated) by UNSW have shown that with good process optimisations, the considerably high conversion efficiencies (7.1%) can be attained (UNSW, 2011).

CHAPTER 3

THEORY

3.1 Photovoltaic Effect

Photovoltaic conversion is a conversion of light energy from the sun to electrical energy by a photovoltaic (PV) cell (i.e. solar cell). The mechanism behind the power generation originates from the ideas of quantum theory. The theory explains that light composed of packets of energy called photons whose energy depends on the frequency or colour of light (Nelson, 2003).

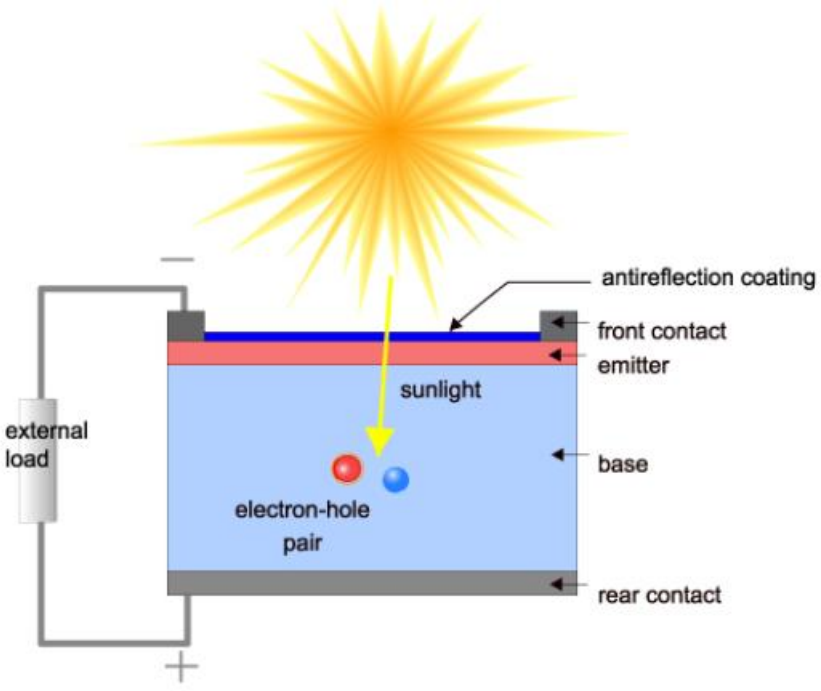

Figure 3.1: Photovoltaic effect in a solar cell.